The influence of mass diffusion on the photothermal signals detected via the mirage effect. II. Experiments

1995 J. Phys.: Condens. Matter 7 9401

(http://iopscience.iop.org/0953-8984/7/49/006)

J. Phys.: Condens. Matter 7 (1995) 9401–9424. Printed in the UK

The influence of mass diffusion on the photothermal signals detected via the mirage effect: II. Experiments

M Z Silva†, Ph Forge and F Lepoutre

Laboratoire d'Optique Physique, ESPCI, 10 rue Vauquelin, 75005 Paris, France

Received 19 June 1995

Abstract. This paper presents the description of a mirage set-up especially developed for the detection of the adsorption of a gas that is condensable close to normal temperature and pressure on a solid sample.

The experiments performed with this set-up are used to test and evaluate the theoretical model established in part I of this work. In order to satisfy the hypotheses of the theory, the solid chosen is a stainless steel sample and the gas chosen is a mixture of chloroform (or dichloromethane) with argon. Within the experimental conditions specified by the model, a good agreement between the measurements and the results of the calculation is found up to the saturation pressure.

These results demonstrate the good sensitivity of the mirage effect to the number of molecules adsorbed in the first layer when multilayer adsorption is reached. They confirm that this method can be used to measure the thermal diffusivity and the mass diffusion coefficient of gas mixtures, as predicted by the model in part I. Experiments performed beyond the condensable gas saturation pressure reveal the sensitivity of the signal to the nucleation–condensation process and to the dynamics of droplet growth on a solid surface.

1. Introduction

In the theoretical part of this paper (part I), a one-dimensional (1D) model was established to calculate the gradients of temperatures and concentrations in a partially condensable gas mixture close to a solid surface periodically heated. The experiment chosen here as being sensitive to these gradients is a mirage effect study. It consists essentially in the measurement of the deflection of a light beam crossing the region where these gradients produce refractive index variations. The objective of this experimental part is to validate the model of part I in order to be able to evaluate the sensitivity of the mirage effect to the adsorption of organic molecules on solid surfaces.

After the description of the main parts of the experimental realization, the experimental conditions and the 'best' solid + gas couple, satisfying as precisely as possible the hypotheses used in the model, will be defined. With these conditions, this couple will be used to compare the experimental results with the predicted behaviours in order to determine the sensitivity of the mirage detection to adsorption processes close to the normal temperature and pressure (NTP) conditions.

The experimental set-up and the procedures are described in section 2. The system was built to check the hypotheses and the conditions of validity of the general expression of the

† Present address: Departamento de Fisica, Universidad do Minho, 4700 Braga, Portugal.

0953-8984/95/499401+24$19.50

mirage deflection established for the periodic regime (frequency f) in the theoretical part of this paper (the notation used is identical in parts I and II):

$$\Phi_n = -(1+\mathrm{i})\frac{1}{n}T_{g_0}\frac{RT_0}{P_0T}\left\{\left[C_A\left(n_A^0-1\right)+C_B\left(n_B^0-1\right)\right]\frac{\mathrm{e}^{-(1+\mathrm{i})(z-l_f)/\mu_g}}{\mu_g}\right.$$
$$-C_B\left(n_B^0-n_A^0\right)\frac{(1-X)(L/RT-1)}{1-X+(1-\mathrm{i})X(\mu_D/2l_g)\left[1+l_g/Y_PRTX\right]}$$
$$\left.\times\frac{\mathrm{e}^{-(1+\mathrm{i})(z-l_f)/\mu_D}}{\mu_D}\right\}. \tag{1}$$

This equation, relying on the hypothesis of 1D diffusion, is composed of two contributions: the thermal wave (produced by the periodic temperature gradient) and the mass wave (produced by the periodic concentrations gradients).

In section 3, the different features which may invalidate the 1D hypothesis will be successively examined. In section 4, the experimental conditions for which either the thermal wave or the mass wave contributions dominate will be chosen in order to measure the heat diffusivity (α) and the mass diffusion coefficient (D) which appear in expression (1) through the thermal (μ_g) and mass (μ_D) diffusion lengths respectively:

$$\mu_g = \sqrt{\frac{\alpha}{\pi f}} \tag{2}$$

$$\mu_D = \sqrt{\frac{D}{\pi f}}. \tag{3}$$

These experimental data (α and D) are used to interpret the experiments described in section 5 in which the mirage deflection is measured as a function of the filling pressure in the cell.

Up to the saturation pressure P_{sat}, it will be shown that the experiments verify the theory rather precisely. In particular, the dominant mass wave contribution at pressures close to P_{sat} is observed to be in very good agreement with the model predictions. But, in a systematic way, one also observes that the experiments can be continued above the saturation pressure. This phenomenon, called supersaturation, will be discussed and qualitatively interpreted.

2. The experimental set-up and procedures

2.1. Organization of the set-up

As explained in the introduction, the set-up described in this section is not optimized to provide the best possible detection of adsorption but to satisfy the hypotheses used to establish the model. The set-up is organized in three parts. The two first parts, as shown in figure 1, concern:

(i) the cell containing the gas mixture and the solid on which the adsorption takes place;
(ii) the system for the preparation and the transfer of the gas mixture to the cell.

The third part which is not represented in figure 1 concerns the optical elements which provide, on the one hand, the modulated beam inducing the periodic gradients close to the sample surface (the pump beam) and, on the other hand, the detection of these gradients via the mirage effect (the probe beam).

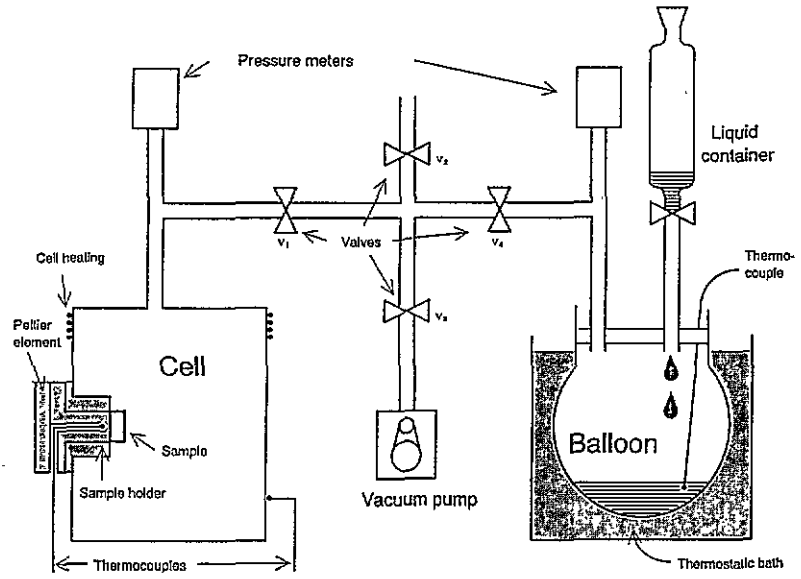

Figure 1. The experimental set-up. The gas is prepared in the balloon by mixing a condensable component (introduced as a liquid and vaporized in the balloon) and a non-condensable gas (introduced by V_2–V_4). V_1 is a needle valve used to fill the cell. The pump and probe beams are not represented. The probe beam direction is perpendicular to the plane of the figure and the pump beam is in the plane of the figure, perpendicular to the sample.

2.2. The cell for the measurements

The solid sample is placed in a closed vessel (see figure 1; the volume is about 10 cm^3) into which, starting from a primary vacuum, the gas mixture is introduced. This cell has three windows—the first one (in front of the sample and parallel to its surface) to allow for the passage of the pump beam, and the other two (on walls perpendicular to the sample surface) for the passage of the probe beam. The whole cell can be moved with respect to the probe beam in order to adjust the surface–probe-beam distance.

The solid specimen is fixed with a heat-conductive glue on a copper holder thermally insulated from the remaining part of the cell. Attached behind this holder, a Peltier element allows the sample to be cooled to a few degrees below the cell wall temperature.

Two versions of this cell which differ only by the positioning of the sample, horizontal or vertical, were used. The horizontal layout is especially important for the study of supersaturation (see section 5.3).

The upper part of the cell can also be heated via the Joule effect. Two thermocouples (precision 0.1 °C) give the temperatures of the cell and the sample. A piezoelectric pressure gauge (range 0–3 bars, precision 1 mbar) measures the total pressure of the mixture in the cell.

2.3. The mirage bench and the pump beam

The principle of the method is to probe the refractive index gradient close to the sample surface via the deflection of a laser beam skimming the surface. The deflection of the probe beam is measured by a quadrant cell protected against the scattered light of the pump by an interference filter.

To reach very low levels of noise, it has been shown [1] that a compact arrangement

which does not suffer from any mechanical deformations is necessary. When the system is not perturbed by global vibrations coming from outside, and if the probe laser has a very low pointing noise, the sensitivity of such a bench is mainly limited by the photon shot noise and can reach 10^{-10} rad $Hz^{-1/2}$ above 60 Hz.

Unfortunately, during experiments taking longer than 30 minutes (such as the ones performed here) He–Ne lasers often present thermal drifts of their direction of emission, so laser diodes are preferable for providing the probe beam in our system. With laser diodes, the pointing noise is larger than the photon shot noise and the sensitivity is limited to about 10^{-9} rad $Hz^{-1/2}$ at a few hundred Hz (frequencies used in these experiments), but the long-term stability is perfect, thus providing a very good reproducibility of the experimental measurements.

More technical details concerning the mirage bench used in these experiments can be found in several papers [2] where the systems used are very similar.

The first source of light tested for the sample heating was an ionized argon laser modulated by an acousto-optic modulator. The power of the laser can be continuously adjusted between 10 mW and 1 W. The modulation frequency is adjustable over a large range (0–20 MHz). The beam is highly monochromatic allowing for a very efficient protection of the quadrant cell from the scattered light.

Despite of these advantages, a filament source (halogen lamp) was finally preferred because it provides a much more uniform illumination of the sample surface and we will see in section 3.2 that a 1D illumination is critical for checking our model. The cross section of the beam at the sample surface is equal to 0.6 cm^2. The power can be adjusted step by step between 40 mW and 200 mW. The intensity is modulated by a mechanical chopper which can operate between 4 Hz and 1 kHz with 100% of modulation. The white light scattered by the sample surface towards the quadrant cell of the mirage bench is stopped by a very narrow interference filter centred on the wavelength of the laser diode.

2.4. *Gas mixture preparation*

The gas is prepared by mixing a non-condensable gas (coming through the valve V_2 in figure 1), and a liquid vaporized in a heated balloon. The temperature and pressure in the balloon are measured by use of a thermocouple and a pressure gauge identical to the ones in the cell.

During the mixture preparation, the adsorption cell and the connecting pipes are emptied. The valves V_3 and V_1 are closed and V_4 is opened. The needle valve V_1 is then opened and two kinds of experiment can be performed:

(i) measurements of mirage amplitude and phase at constant gas pressure (P) as functions of the modulation frequency (f), probe–surface distance (z) or cell temperature (T); and

(ii) measurements of mirage amplitude and phase as functions of P (the speed of the gas admission being controlled by the needle valve V_1) for different chosen values of f, z and T.

In all of these experiments, the general thermodynamic equilibrium is never reached. This is obvious when the measurements are performed during the progressive filling of the cell since a gradient of pressure is always present during the experiment. It is also the case at constant pressure since it is necessary to keep the sample at a temperature a little bit lower than that of the remaining parts of the cell to achieve a preferential adsorption/condensation on the specimen surface. Nevertheless, it can be assumed that very close to the sample

surface (i.e. precisely where the skimming beam probes), a local equilibrium exists, and it will be one of the goals of the experiments to check whether or not this hypothesis is practically realized with this mirage technique.

Finally, the photoelectrical signal delivered by the quadrant cell of the mirage bench is demodulated by a lock-in amplifier. For all the experiments, the amplitude and the phase of the mirage deflection and the adjustable parameters (temperatures, pressures, modulation frequency, probe–surface distance) are recorded as functions of time, and the operator can choose the more convenient presentation of the results (amplitude or phase as functions of one of the adjustable parameters). Finally, to achieve an easy comparison between theory and experiments, the curves are sampled prior to obtaining a mathematical best fit with the calculated curves.

3. Model limitations and sample selection

3.1. Hypotheses

Three hypotheses used to establish the model have to be satisfied by the physical properties of the sample–gas couple and by the experimental conditions before any investigations of the adsorption phenomenon itself can be performed:

(i) the diffusion processes should be one dimensional;

(ii) the mirage deflection should be produced only by the gradients of the gas refractive index and not by the thermoelastic deformations of the sample;

(iii) the optical absorption of the pump beam should take place almost at the surface of the specimen.

Indeed, it has been shown in many papers [3] that the non-validity of only one of these conditions is sufficient to affect the interpretation of the classical thermal mirage effect using a simple 1D theory [4] similar to the one developed in part I. And moreover, in our more complex case, these conditions must be strictly fulfilled if we want to be able to understand the contribution of the adsorption and desorption to the mirage signal.

3.2. Three-dimensional effects

The model assumed that the diffusion processes take place only along the z-axis, perpendicular to the surface. This is true if the pump-beam radius is large enough to be considered as uniform on the sample surface, i.e. if it does not generate important lateral temperature gradients in the material. It is also necessary to have the detection as localized as possible, i.e. to have a very thin probe beam. Of course, these two requirements cannot be fulfilled rigorously and so it is important to determine the limit values of r_p (the pump-beam radius) and r_s (the probe-beam radius) for which the 1D model is a good approximation.

In a general way, we have observed experimentally that the three-dimensional (3D) effects on the thermal and on the concentration contributions have the same orders of magnitude. To simplify the study of the 3D perturbations, our discussion is limited to the changes produced in the thermal effect, assuming that the limitations thus deduced will be also valid in the general case of simultaneous thermal and concentration contributions.

We start with the finite-probe-beam effect. This effect is rather easy to take into account since it is sufficient to convolute the result from expression (1) obtained for $r_s = 0$, with the gaussian distribution of the laser used. We recalled in part I of this paper that the result of this operation is a simple product of the z-dependent terms with a factor which is written

for the thermal contribution as

$$\exp\left(\frac{\mathrm{i}\, r_s^2}{2\mu_g^2}\right) \operatorname{erfc}\left(\frac{(1+\mathrm{i})\, r_s}{2\sqrt{2}\,\mu_g} - \frac{\sqrt{2}\, z}{r_s}\right). \tag{4}$$

erfc is the complementary error function.

This expression shows that the effect of the finite radius r_s increases with the ratios r_s/μ_g and z/r_s, i.e. is more important at large frequencies and with a probe beam close to the surface. Anyway it should be noticed immediately that, practically, the probe-beam radius cannot be reduced below 30 μm since for smaller values the divergence of the beam at the focused point above the sample becomes too large with respect to the sample radius and a significant part of the beam is then hidden by the sample.

The multiplicative term (4) was introduced in the general expression for the thermal contribution and the main result of this correction is that the phase is more modified than the amplitude. These modifications are also more important when the beam is closer to the surface and the frequency is higher: for instance, at 900 Hz, the phase shifts between calculations performed without and with convolution, for a 50 μm probe-beam radius, are equal to 20° at $z = 50$ μm and to 2° at $z = 200$ μm.

The second 3D effect is due to the finite pump-beam size which produces temperature gradients parallel to the surface and thus lateral diffusions of both heat and molecules.

To prevent such effects, the pump beam should illuminate the sample surface as uniformly as possible. But in practice an increase of the pump-beam radius r_p is equivalent to a signal decrease since it is well known that the 3D signals are inversely proportional to r_p [5]. Thus a compromise between a good signal-to-noise ratio and the limit of validity of the model should be researched.

We have compared the results of the calculations performed with a uniform illumination and gaussian beams of radii larger than 1 mm in the case a purely thermal effect. For all the radii tested, the differences appear only at low frequencies (below 100 Hz). These discrepancies are more important when the probe is closer to the surface and when the ratio of the thermal diffusion lengths in the solid and in the gas (μ_s/μ_g) is smaller, i.e. for bad heat conductors. Such a result has also been discussed by other authors [6]. In the conditions of the experiments described in the following sections, the pump-beam size effect can always be considered as negligible for gaussian beams of radii r_p larger than 1 mm.

3.3. Thermoelastic deformations

The absorption of the pump produces not only an increase of the surface temperature but also a photoelastic deformation. Since the shape of the probe beam is gaussian, its extension is infinite and, no matter what value its radius (r_s) takes, there it always exists a small part of the beam which is in contact with the surface and thus is deflected by the thermoelastic deformation [7].

This effect is easily detected with our system: it is just necessary to empty the cell. The periodic displacements of the beam can then only be attributed to the thermoelastic deformations.

In vacuum this effect decreases very quickly when the probe–surface distance z increases. This result is confirmed experimentally in air where discrepancies with respect to the thermal model and due to thermoelastic deflection appear only at small distances z (see figure 2). Far from the sample surface, the linear dependences (on z or $\sqrt{f}$) are recovered and lead to a good value of the thermal diffusivity of air, confirming that the thermoelastic

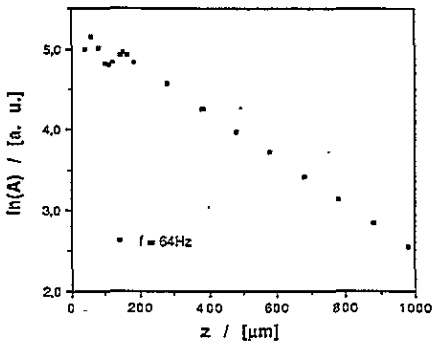

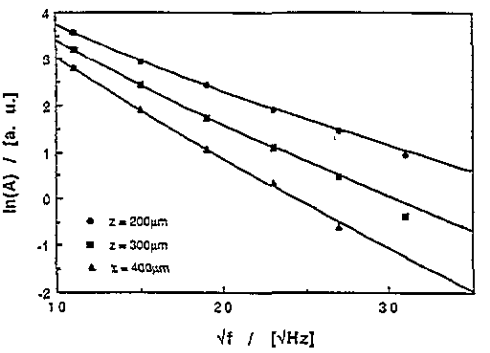

Figure 2. The amplitude and phase of the mirage signal in air as functions of the probe-beam–sample surface distance z. The effect of the thermoelastic deformations appears for the lowest values of z. Sample: black polymer, $r_p = 5$ mm, $r_s = 50$ mm. The air was at NTP in the cell.

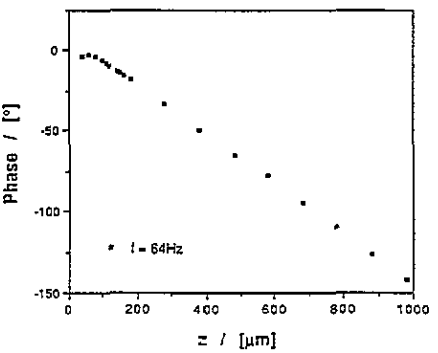

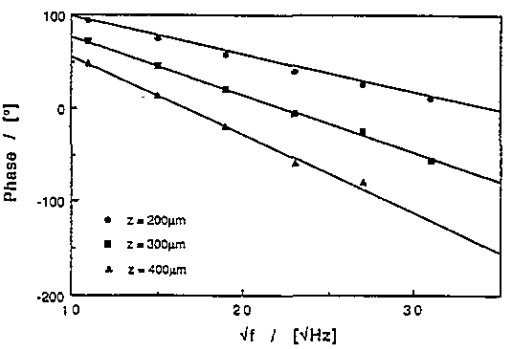

Figure 3. Experimental values of the mirage amplitude and phase in air for a semi-transparent material ($\beta = 10^{-3}$ m^{-1}) as functions of $f^{1/2}$. The full curves are obtained from a best fit between these experimental points and a calculation taking into account the in-depth absorption of the pump.

contributions are then very small. Typically, for all the samples used the thermoelastic signal was always found to be negligible at distances z larger than 200 μm.

3.4. In-depth optical absorption

Except the metals, all the materials absorb the visible light in depths larger than 1 μm. Unfortunately the photothermal signals are inversely proportional to the thermal conductivity and so are weak in metals. It is often interesting to choose a bad conductor as the polymer to increase the signal-to-noise ratio. In such a case, it is important to recognize the domain of the experimental conditions in which the in-depth optical absorption does not affect the results deduced from the assumption of a surface absorption too much.

As for the 3D effects, we have limited this study to the case of the thermal contribution alone. The data for the optical absorption (β) of a semi-transparent black glass sample ($\beta = 10^{-3}$ m^{-1}) are introduced in the calculation of the mirage thermal deflection and compared to the case where a surface absorption is assumed in a sample of identical thermal properties.

The general result of this calculation, confirmed by experimental observations, is that the in-depth absorption does not modify the dependences of the amplitude and phase on the probe–surface distance z but strongly affects the dependences on the frequency (see figure 3).

The variations of the amplitude and phase as functions of the distance z, which are kept linear with a semi-transparent sample, lead to an exact value of the thermal diffusivity even if the optical absorption coefficient is unknown. In contrast, the dependences on the square root of the frequency are no longer linear as they were for an opaque material. Of course, if the thermal parameters of the sample are known, a best fit with a theory taking into account the in-depth absorption (such as the one presented in figure 3) will restore the value of β. But the most interesting result for our study is that this non-linear dependence is a good test for discovering a semi-transparency in an unknown material. A material will be considered as opaque in our experiments if the variations with $\sqrt{f}$ are linear within the experimental uncertainties.

3.5. The effect of the DC temperature increase

Up to now we have assumed that the DC temperature of the sample is the same as that of the copper holder. Actually the modulated excitation also leads to a DC heating which can be evaluated by assuming that there are no heat losses at the front surface and a temperature T_0 imposed at the rear surface. For a sample of conductivity k_s and thickness l_s, the continuity of the heat flux gives an increase ΔT of the front surface DC temperature given by

$$\Delta T = \frac{Q_0 l_s}{2k_s} \tag{5}$$

where Q_0 is the power absorbed by unit surface at the sample surface.

This expression shows that the use of strongly absorbing materials or/and thick bad conductors can lead to rather important increases of the DC temperature (for instance, $\Delta T = 1$ °C for 1 mW mm^{-2} absorbed on a sample 1 cm thick with $k_s = 5$ W m^{-1} K^{-1}). This increase of the sample DC temperature produces an increase of the gas DC temperature in the vicinity of the surface and, since both the refractive index and the diffusivity of the gas are temperature dependent, it induces a change in the mirage deflection (non-linear effects).

It has been shown [8] that an increase ΔT of 3 K produces, in air, variations of the mirage amplitude and phase respectively equal to 1% and 1°. This result gives the order of magnitude of the absorbed power that must not be exceeded to keep the influence of these non-linear effects on the mirage signal in the ranges 1% in amplitude, 1° in phase: less than 1 W mm^{-2} for a 10 mm thick bright metallic sample, less than 1 mW mm^{-2} for a black polymer sample 10 mm thick.

3.6. The choice of the solid–gas couple

Before choosing the material of the solid specimen, we have to define its geometry. For the sake of simplicity the samples are cylindrical (cross section diameter d).

The signal is proportional to the absorbed power per unit surface, i.e. in our case of uniform illumination inversely proportional to d^2, and to the length of interaction between the probe and the heated surface which is equal to d in the case of a complete illumination of the sample surface. Thus the signal is proportional to d^{-1} so d should be chosen as small as possible. In addition, a small value of d leads to a better focusing of the probe beam above the sample and thus a smaller probe–sample distance z which increases the signal

too. In our set-up, the physical limit of d is given by the smallest diameter of the pump beam (filament source) that can be achieved in the plane of the sample holder ($\approx$10 mm, see section 2.3).

Concerning the sample thickness l_s, we saw in section 3.5, expression (5), that the sample should be thin enough to avoid an increase of the sample DC temperature, which is proportional to l_s. On the other hand, we also observed experimentally that the sample thermoelastic deformations increase when the sample is thin, whatever the quality of the gluing on the holder. For metallic samples, this effect becomes important, at the usual working distances z, for $l_s < 2$ mm and this limit value was chosen for all the samples. Let us note that $l_s \approx 2$ mm is also compatible with the theoretical requirement (included in the model) that the sample has to be thermally thick ($\mu_{th} < l_s$) at the modulation frequencies used in the experiments.

Concerning the choice of the material itself, the results of the previous sections show that the signal increases when the sample is more optically absorbing and less thermally conductive. But we also saw that there are limitations due to the emergence of thermoelastic deformations (section 3.3) and to non-linear effects (section 3.5). Since it is difficult to give *a priori* values for these effects, the material itself was selected by testing the linear dependences of the amplitude and phase of the purely thermal mirage signal as functions of the distance z and the square root of the frequency, $\sqrt{f}$, in argon (argon was preferred to air because its purity is much better defined). All these linear dependences should lead to the same value of the thermal diffusivity of argon (actually with different precisions, as will be discussed in section 4). In addition, this test ensures that no 3D or semi-transparency effects are important. Two samples were selected in that way: a metal chosen for its low conductivity, stainless steel ($k_s = 13.8$ W m^{-1} K^{-1}), and an oxide chosen for its large optical absorption, TiO_2. These two materials satisfy the previous tests. For a given value of the pump power, the oxide produces much larger signals than the metal since its optical reflectivity and its thermal conductivity are smaller, but its surface is porous—which is not included in our model of adsorption. Finally TiO_2 is only kept for qualitative information and the main parts of the experiments are done with the stainless steel sample.

The gas mixture was always prepared with high-grade argon in order to prevent any pollution—in particular by water steam. The condensable gas is chosen following the results published by previous authors [9, 10]. Among all the possible organic gases condensable in conditions close to NTP, three molecules were selected (dichloromethane CH_2Cl_2, chloroform $CHCl_3$, and acetone C_3H_6O) for their large refractive indexes which increase the amplitude of the mass wave (see the factor $(n_B^0 - n_A^0)$ in expression (1)), allowing for a clear interference between the two contributions during the cell filling.

4. Determination of the gas diffusion parameters

4.1. Thermal diffusivity of the gas mixture

The thermal diffusivity of a mixture of two gases A and B is given by

$$\alpha_g = \frac{k_g}{\rho_g c_{pg}}. \tag{6}$$

If ρ_g and c_{pg} are deduced via elementary relations from the values $\rho_{A,B}$ and $C_{pA,pB}$ of the gases A and B (see relations (50) and (51) of part I), the relation between k_g and k_A, k_B makes use of parameters for interactions between the molecules A and B which are generally not well known. A rough estimate of k_g can be deduced from relation (49) of part I, but an experimental measurement would be preferable if its precision were satisfactory.

As was explained in section 3 of this part, when the mirage signal is purely thermal and when the hypotheses of the model are fulfilled, the measured value of α_g can be easily deduced from any of the linear variations of the logarithm of the amplitude ($\ln(A)$) or of the phase (φ) with the square root of the frequency ($\sqrt{f}$) or with the probe–surface distance (z). We have verified that the most precise method is a linear regression on the experimental points giving $\varphi(z)$.

When non-condensable gases are used, the thermal diffusivities deduced from these measurements are in agreement with literature data within a precision of a few per cent. But with a mixture containing one condensable gas, systematic errors are observed: for instance, the thermal diffusivity of a mixture of 10% of N_2 with 90% of acetone is found to be equal to 2.2×10^{-4} m^2 s^{-1} at 312 K while expression (49) of part I and the literature data lead to 2×10^{-5} m^2 s^{-1}.

Of course, such a difference cannot be attributed to experimental uncertainties or to the imperfection of relation (49). Actually, this discrepancy is due to a partial condensation of B in the pipes connecting the balloon to the cell during its filling. For instance, for the mixture presented above, it would be necessary to assume a concentration in B of only 57% to recover the literature data. To reduce this effect, it is necessary to heat the pipes used for transfer to a few °C above the cell temperature. But even with such precautions, the determination remains imperfect and these 'thermal' measurements are used to determine the exact value of the concentration (X) in the cell instead of α_g which is deduced from the literature data and expression (49) of part I.

4.2. The mass diffusion coefficient of binary gas mixtures

To verify our model, it is also necessary to know the diffusion coefficient D for diffusion of the two gases A and B of the mixture.

Very few measurements of D have been published, and to check the method which is described in this section, it is necessary to choose a mixture for which data are available in the literature. The chosen gas is a mixture of argon and acetone. Let us recall that D is almost independent of the mixture concentration, so the problem mentioned in section 4.1 is not important here.

We saw in the previous section that when the thermal contribution dominates, the variations of $\ln(A(z))$ and $\varphi(z)$ are linear. These linear behaviours are still present when in contrast it is the mass contribution which dominates. Indeed in expression (1), the second term (the concentration wave) exhibits a linear dependence on z similar to that of the first term (the thermal wave).

The procedure used to measure D is then the following one:

(i) a mixture is prepared in the balloon and progressively admitted into the cell previously emptied;

(ii) as the pressure increases in the cell, the amplitude and the phase of the mirage signal are recorded (see figure 4). At low pressures, the signal is dominated by the thermal contribution. When the pressure increases, the amplitude of the concentration wave increases and the phase rotates slowly until it reaches a new value corresponding to the predominance of the second term of expression (1) (see the final part of the curves in figure 4, for $P \geqslant 24$ kPa). Then the cell is closed and the phase of the signal is recorded as a function of the distance z. The slope of the linear dependence obtained is equal to the inverse of the diffusion length $\mu_D = \sqrt{D/\pi f}$.

Figure 5 gives an example of such measurements at different frequencies. All the slopes

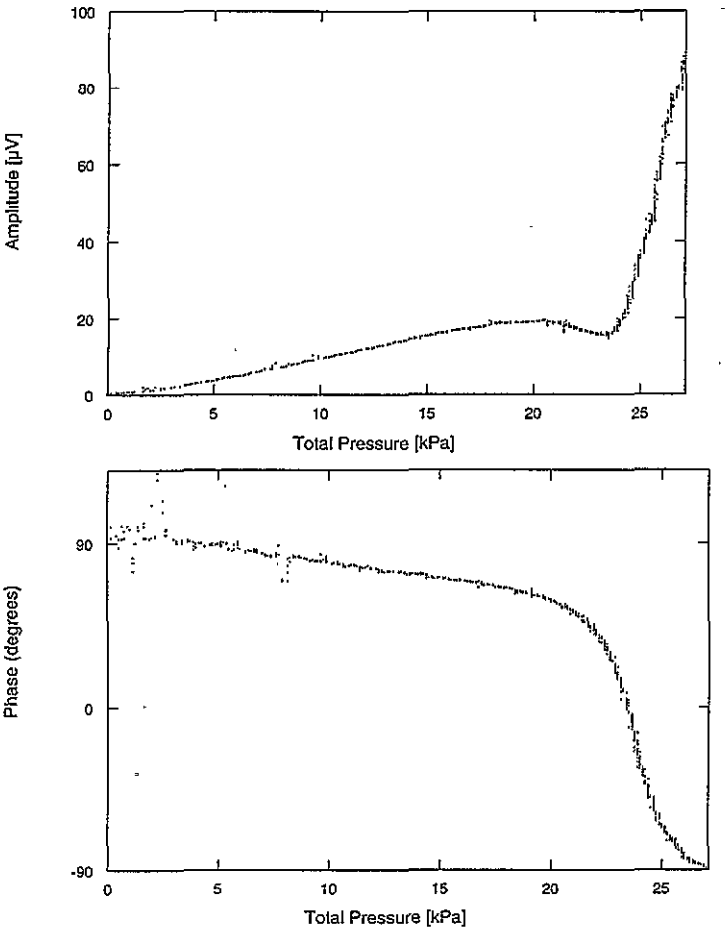

Figure 4. The amplitude and phase of the mirage signal as function of the total pressure in the cell. Gas mixture: acetone ($X = 0.9$) + argon. Solid: stainless steel. $T = 294$ K, $z = 190$ μm, $f = 121$ Hz.

lead to the same value of D ($D = (3.7 \pm 0.1) \times 10^{-5}$ m^2 s^{-1} at $P = 30$ kPa and 281 K). The data for the mixture of air (or argon) and acetone give $D = 11.26 \times 10^{-5}$ m^2 s^{-1} at $P = 100$ kPa and 293 K. At this pressure, $P = 100$ kPa, our measurements correspond to $D = (11 \pm 0.3) \times 10^{-5}$ m^2 s^{-1} in good agreement with the data. This procedure is systematically followed for the other mixtures used in the measurements described in section 5.

5. The mirage signal as a function of the total pressure

5.1. The qualitative approach

Although it is theoretically possible to modify the respective influences of the thermal and mass contributions to the signal by changing parameters such as the modulation frequency, the temperature (see for instance figure 7 of part I) or the mole fraction of the condensable gas at constant total pressure, we found that the easiest way of achieving this result is by varying the total pressure in the cell.

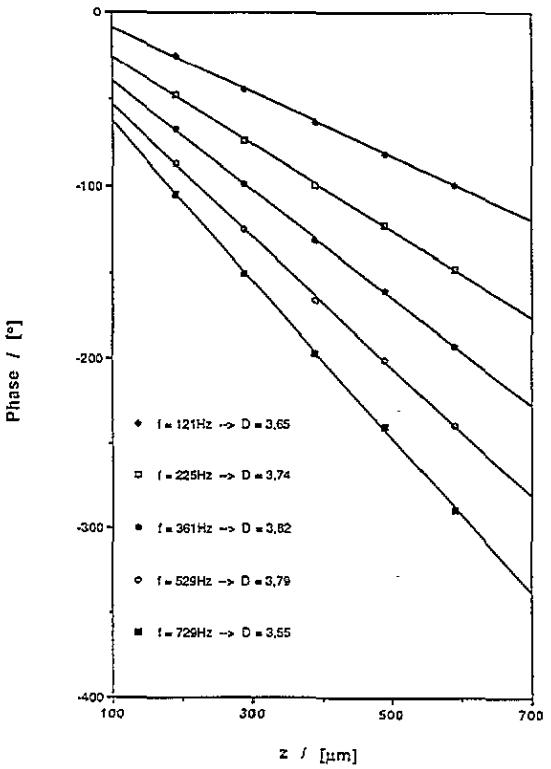

Figure 5. Experimental measurements of the phase as a function of the probe–surface distance z. The mass diffusion coefficient D of the mixture (acetone ($X = 0.9$) + argon) is deduced from the slopes of the linear regressions at various frequencies. (The D-values are 10^{-5} m^2 s^{-1}.)

An example of these variations with the total filling pressure P is given in figure 4. At low pressures and up to 20 kPa, the amplitude is small and increases slowly. Similarly, the phase varies slowly from about 100° to 90°.

Then, between 20 and 24 kPa, the amplitude decreases and the phase undergoes a sharp variation of almost 180°.

Above 24 kPa, the amplitude increases very quickly and the phase is stabilized to a value close to −90°.

Such behaviour, in very good qualitative agreement with the model, is characteristic of the transition from the thermal regime to the mass regime:

(i) at low pressures, the signal is only due to the thermal contribution; as explained in section 3.2 of part I, the amplitude of the thermal contribution increases with the pressure in the range of frequencies and sample–probe distances usually chosen to have a good signal-to-noise ratio (in figure 4, $f = 121$ Hz and $z = 190$ mm)—for the same conditions, the phase of the thermal contribution decreases slowly [9];

(ii) therefore, the amplitude decrease observed above 20 kPa can only be attributed to the second term of expression (1) which starts to compete with the thermal term at that pressure—since the two terms of expression (1) have opposite signs, this competition is expressed as a decrease of the total amplitude; at 24 kPa, the two contributions have similar magnitudes and a minimum occurs.

The value reached by this latter minimum depends upon the respective phases and amplitudes of the two terms: it is a real interference so, depending upon the conditions,

either the amplitude falls to almost zero and an exact phase shift of 180° is observed, or the competition is reduced to a simple inflexion of the amplitude. A change of one of the experimental conditions or, within the same experimental conditions, a change of one element of the solid–gas couple can considerably modify the shape of the curves of amplitude and phase as functions of P. This result which is illustrated by a comparison between figures 4 and 6 explains why in some previously reported photoacoustic experiments [9, 10] the introduction of volatile molecules decreases the photothermal signal instead of increasing it as had been expected by the experimenters. Since the conditions for the two experiments of figure 4 and 6 are totally identical except that the condensable gas is acetone for figure 4 and chloroform for figure 6, it is interesting to use equation (1) to see what the main parameter which acts so efficiently on the mass contribution is. A numerical evaluation of this second term shows that, in a first approximation, it is proportional to Y_P. Using the BET model [11, 12] to describe the process of adsorption, Y_P is given by equation (41) of part I which can be written as

$$Y_P = \frac{Y_1 f(P_B/P_{sat})}{P_{sat}} \qquad (7)$$

in which $f(P_B/P_{sat})$ increases quickly when the partial pressure of the condensable gas approaches the saturation ($P_B \rightarrow P_{sat}$) and Y_1 is the number of moles adsorbed per unit surface of a monolayer.

Following this approximation, the second term of (1) is the larger when Y_1 is large, P_B close to P_{sat}, and P_{sat} small. In the cases of figures 4 and 6, it is clear that the mass contribution is more important with acetone than with chloroform. Since the saturation pressure of acetone is larger than that of chloroform, this increase of the mass contribution in the case of acetone can only be attributed to a larger value of Y_1.

As was explained in section 2.2, the sample holder is cooled by a Peltier element in order to improve the adsorption on the solid specimen. This influence of temperature on the adsorption process is due to the temperature dependence of P_{sat}: it is well known that P_{sat} increases with T, so Y_P decreases when T increases (see expression (42) of part I). This temperature effect is clearly observed in figure 7 where ΔT is the temperature difference between the temperature used to prepare the mixture and the sample temperature:

(i) when the sample holder is not cooled, the DC temperature is 2 °C larger than the ambient temperature because of the DC pump heating (see section 3.5). Y_1 is too weak to produce a mass contribution larger than the thermal contribution and, at the end of the experiment, the phase shift is much smaller than 180°;

(ii) for $\Delta T = -3$ °C, the minimum of the amplitude and the phase shift of 180° are almost reached but preponderance of the mass contribution is still not observed;

(iii) finally, it is necessary to impose $\Delta T = -6$ °C to obtain a large mass contribution which is revealed, after the minimum, by the sharp increase of the amplitude and the stationary value of the phase at −180° below its value at low pressures.

It is interesting to note that the minimum of the amplitude and the rotation of the phase occur at smaller and smaller pressures as the sample temperature decreases. Since the thermal contribution varies very slowly with the temperature, this displacement of the minimum with temperature is direct proof of the progressive increase of the mass contribution as the sample temperature is decreased.

It is difficult to go further into the comparison with the model using the experimental curves as they are presented in figures 4 and 6. These curves are made up of more than 2000 points from measurements and a mathematical fit with the model is thus too time consuming.

In order to improve the quantitative comparison between theory and experiments, averaging and linearization are performed on the successive points to transform the experimental results into a continuous variation which is then made discrete once again but, this time, with only 50 points, regularly spaced out in pressure. The result of such an operation is shown in figure 8 for the experiment of figure 4 (note that the amplitude is now represented on a semi-logarithmic scale). In such a representation of the experiment, a best fit with the theory is then easy and fast and allows one to find quantitative values which are in agreement with the measurements.

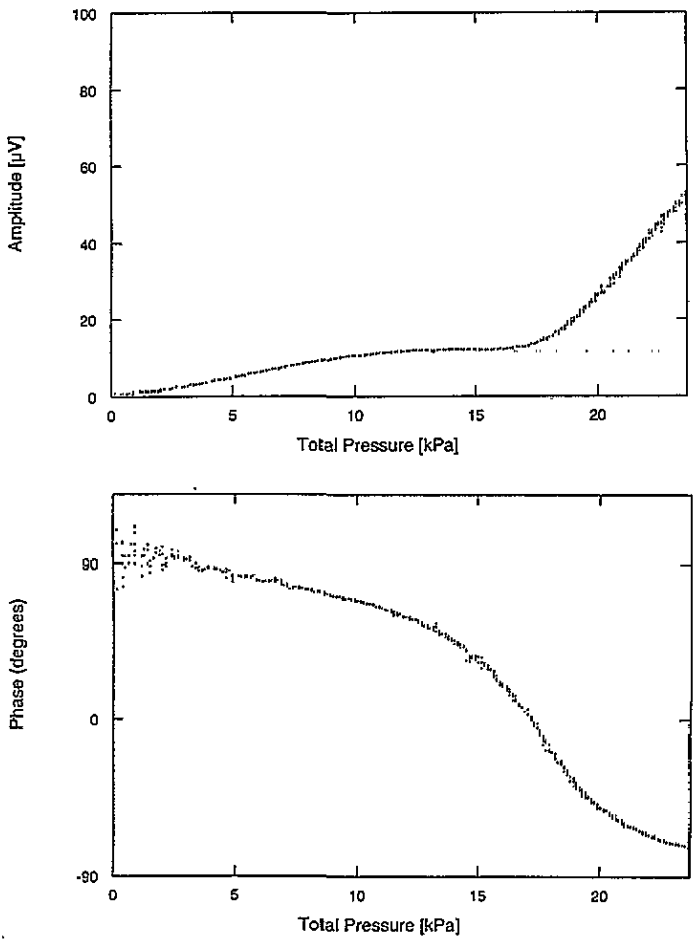

Figure 6. The same experiment as in figure 4 except that the gas mixture is now chloroform ($X = 0.9$) + argon.

The next section examines the quantitative influences of the main parameters Y_1, T, X, and l_f the adsorbed film thickness, and finally leads to evidence of a new phenomenon (i.e. one which is not taken into account in the model) called supersaturation.

5.2. Quantitative analysis

The first question which we have to answer in the framework of a quantitative analysis is: 'Is the mirage effect sensitive to the physics of adsorption, i.e. to the model which describes

the adsorption process?' We have recalled in part I that the different theories modelling the adsorption only differ at low pressures, i.e. for below P_{sat}, where they describe the deposition of the first layer on the solid surface. At pressures close to P_{sat}, all the theories predict almost the same behaviour of Y as a function of the ratio P/P_{sat}. The BET model [12] itself describes the different processes of adsorption of the first layer in terms of the parameter C_1 (see expression (40) of part I) which is related to the difference between the heats of adsorption and vaporization.

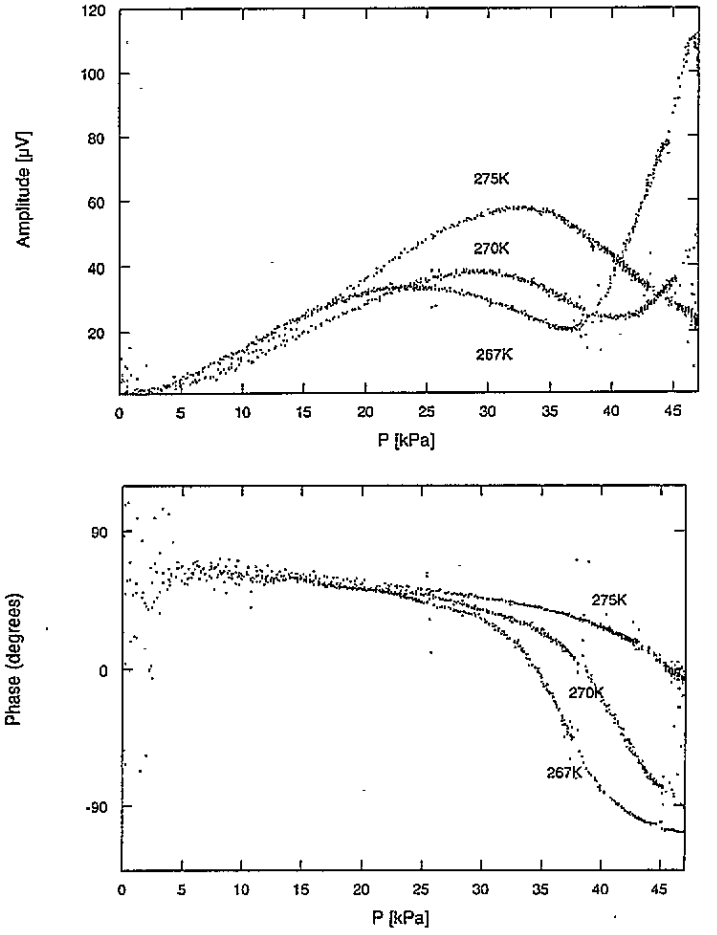

Figure 7. The effect of the sample temperature on the amplitude and phase variations with the total pressure of a mixture of dichloromethane ($X = 0.9$) + air. $z = 210$ mm, $f = 40$ Hz.

Since we saw in the previous section that the thermal contribution is always dominating over the mass contribution at low pressures, the answer to the question is NO! Unless an artifice can be found to reduce the thermal contribution considerably, the mirage effect method is unable to explore the deposition of the first layer and so is unable to test the model of adsorption. This negative result can be verified directly with expression (1): if C_1 is varied with respect to Y_P over its full range (0 to 1), no differences appear in the calculated amplitude and phase of the mirage signal. We confirmed our conclusion about the insensitivity of this method to the adsorption of the first monolayer by replacing the BET

equation (equation (40) of part I) with another model of adsorption: for instance, on using the Frankel–Halsey–Hill equation [12] with appropriate numerical values for the adjustable parameters of the model, no difference in the pressure dependence of the mirage effect is revealed.

Despite this insensitivity to the first-layer deposition, the signal should be highly sensitive to Y_1, the number of moles per unit surface adsorbed in a monolayer (see the previous section). In figure 8, this parameter is varied from 10^{-4} to 10^{-6} mol m^{-2}. The best fit is clearly obtained for $Y_1 = 10^{-5}$ mol m^{-2}. An increase of Y_1 displaces the minimum of the amplitude and the phase rotation in a very sensitive way, as was suggested in the qualitative approach (see section 5.1).

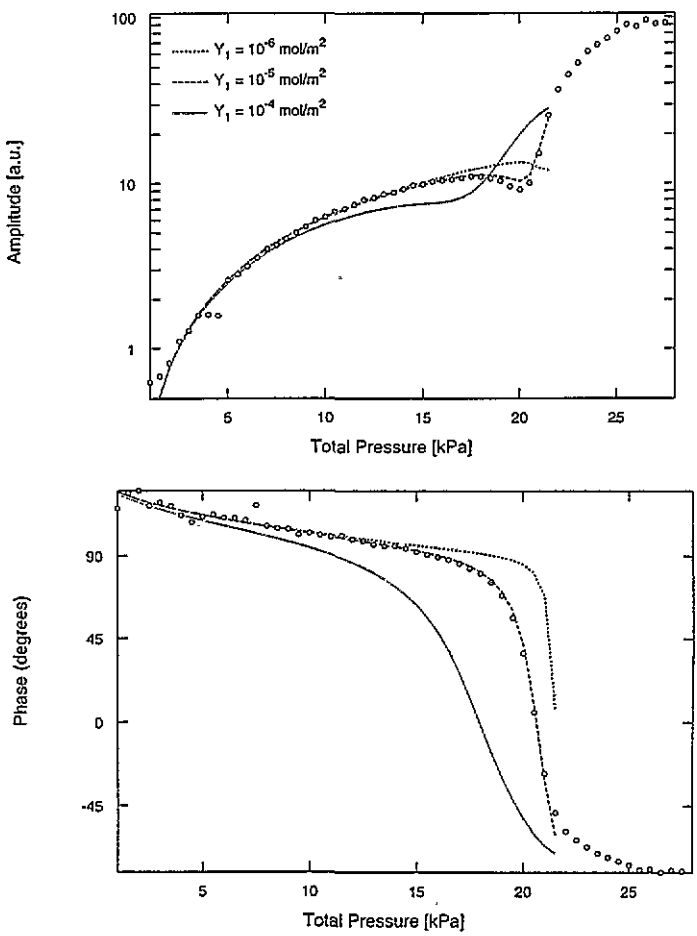

Figure 8. The discretization of an experimental result (acetone ($X = 0.85$) + argon, $T = 287$ K, $z = 190$ mm, $f = 121$ Hz) and the best fit with the model, using $c_1 = 1$, $l_f = 0.1$ μm and Y_1 as the adjustable parameter.

Of course, knowledge of parameters other than Y_1 is necessary to obtain this result—especially the values of the sample temperature (T), the mole fraction of the condensable gas (X) and the thickness of the adsorbed film on the solid surface (l_f).

The first cause of error comes from the not very precise knowledge of the molar fraction of B (X), since we saw that, despite the heating of the pipes between the balloon and the

cell, a proportion of B condensed there. In figure 9, we compare the result of the calculation made using the experimental value, $X = 0.9$ (see section 4.2), with the one giving the best fit with the experiment ($X = 0.85$). From this result we may conclude that the quantity of molecules condensed in the pipes can vary slightly from one experiment to another, modifying in this way the mole fraction X in the cell. This happens especially when using different flow rates while filling the cell.

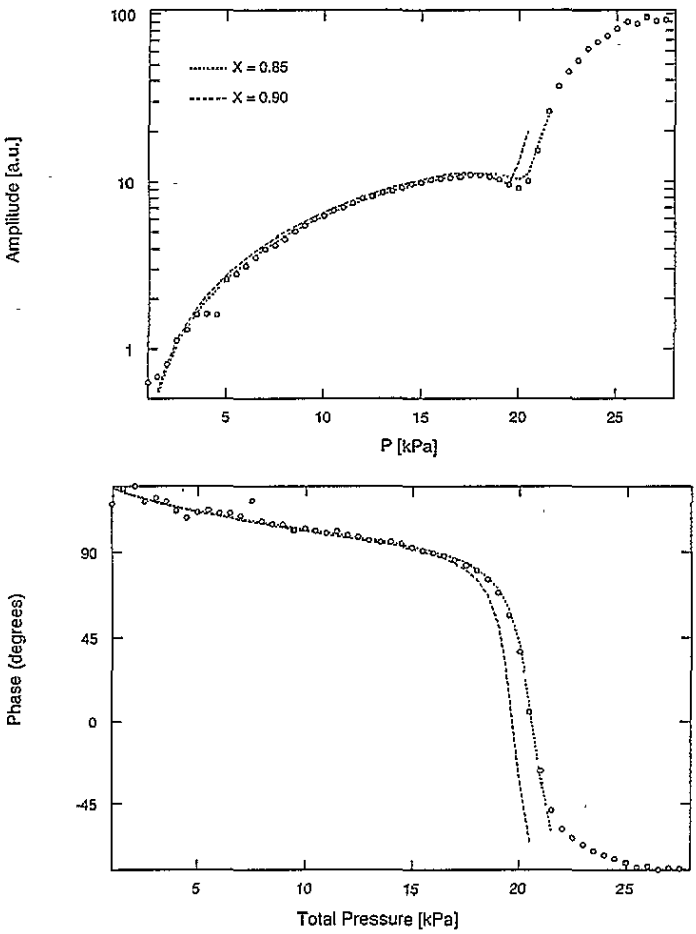

Figure 9. The best fit with the experimental results of figure 8. The adjustable parameter is X ($Y_1 = 10^{-5}$ m^2 s^{-1}, $c_1 = 1$, $l_f = 0.1$ μm, $T = 287$ K, $z = 190$ mm, $f = 121$ Hz).

An error of the same order of magnitude is produced by the uncertainty in the sample temperature (experimentally $\Delta T = \pm 0.5$ °C). In figure 10, T is changed from 286 K to 288 K and the best fit is obtained with $T = 287$ K, the measured value.

Anyway, it is interesting to note that the variations of X and/or T do not modify the signal versus the pressure in the same way as the Y_1-variation does, so, normally, there is no ambiguity about the value found for Y_1.

The main conclusion deduced from the excellent agreement observed between the model and the experiment is that the mirage beam is close enough to the surface to probe a solid–gas couple which is in a local equilibrium, although such an equilibrium does not exist over the whole cell.

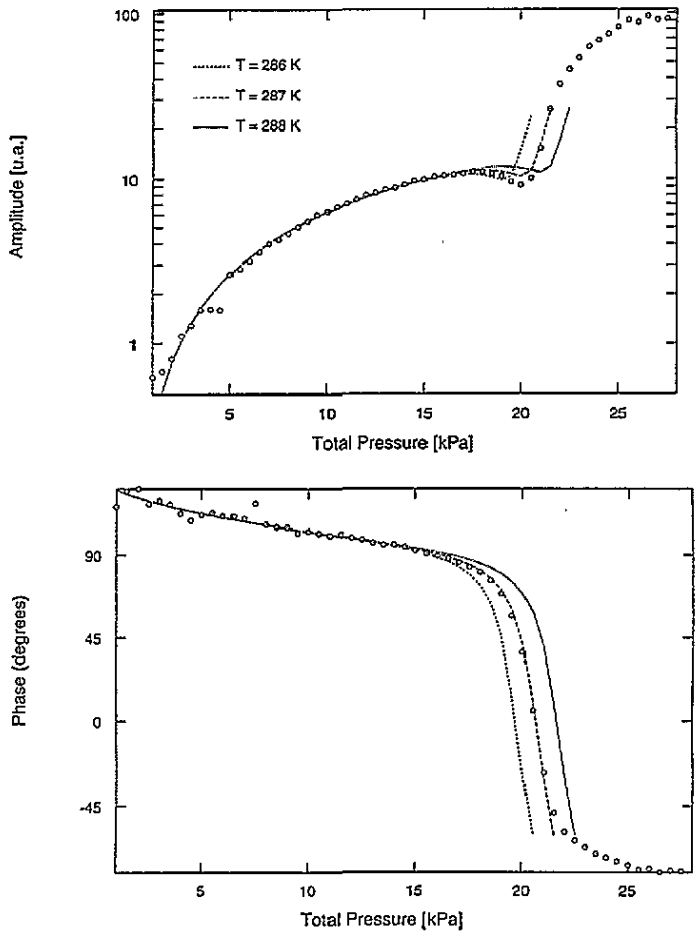

Figure 10. The best fit with the experimental results of figure 8. The adjustable parameter is T ($Y_1 = 10^{-5}$ m^2 s^{-1}, $c_1 = 1$, $l_f = 0.1$ μm, $T = 287$ K, $z = 190$ mm, $f = 121$ Hz).

5.3. Supersaturation

The last unknown parameter is the film thickness l_f. As it is written in relation (I), it appears clearly that l_f acts on the signal via the exponential terms e^{-l_f/μ_g} and e^{-l_f/μ_D}, but l_f is also present implicitly in T_g^0 (the gas temperature at $z = 0$) where it acts via the exponential e^{-l_f/μ_f} (see section 2.2 of part I, especially relation (38)). Since at a given frequency, μ_f is always much smaller than μ_g or μ_D (at the frequency corresponding to figure 8, $\mu_f = 15$ μm, $\mu_g = 230$ μm and $\mu_D = 320$ μm), it is e^{-l_f/μ_f} which produces the sensitivity to l_f observed in figure 11: an evaluation of e^{-l_f/μ_f} immediately shows that as soon as l_f becomes larger than $10^{-2}\mu_f$, the signal decreases by 1%. Therefore, with the data of figure 8, the sensitivity to l_f starts above 0.1 μm.

Using the values of Y_1, X and T deduced from the best fit, we find that only negligible values of l_f are compatible with the experimental results, as is revealed in figure 11. This result is quite surprising: indeed, a film thickness smaller than 1000 Å seems to be incompatible with the fact that we only detect the adsorption when the number of adsorbed molecules per unit surface is very large. For this reason, it is highly improbable that the

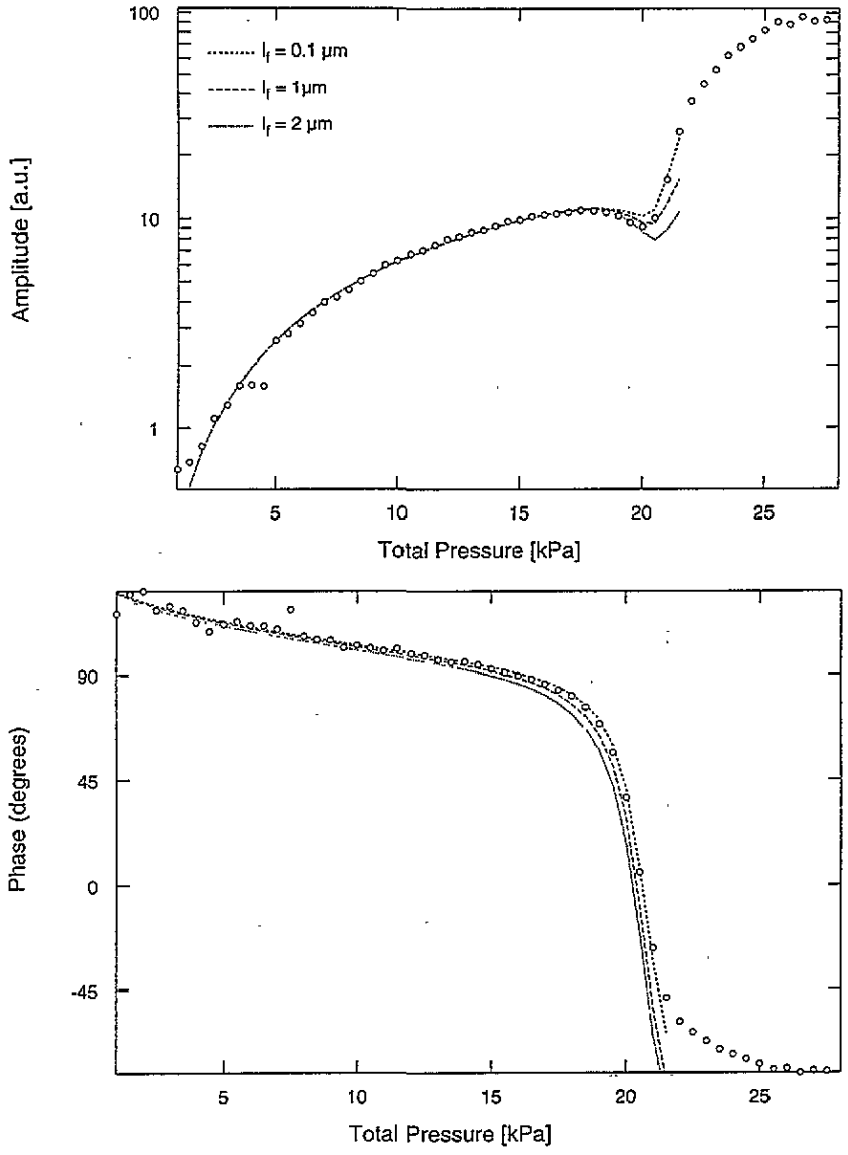

Figure 11. The best fit with the experimental results of figure 8. The adjustable parameter is l_f ($Y_1 = 10^{-5}$ m^2 s^{-1}, $c_1 = 1$, $l_f = 0.1$ μm, $T = 287$ K, $z = 190$ mm, $f = 121$ Hz).

adsorbed molecules are deposited on the surface as a continuous film.

We found that instead of a continuous film the adsorbed molecules deposited on the surface form microscopic droplets. This explains the need for negligible values of l_f to fit the experimental results. In fact, the periodic adsorption–desorption giving rise to the mass contribution to the mirage signal takes place mainly at the triple points where the solid, the liquid and the gas coexist, i.e. at the meniscus of the droplets on the surface. This same phenomenon was demonstrated recently in a very interesting experiment [13].

By waiting long enough after the introduction of the gas mixture into the cell we were able to see, on the surface of the solid sample, macroscopic drops continuously growing

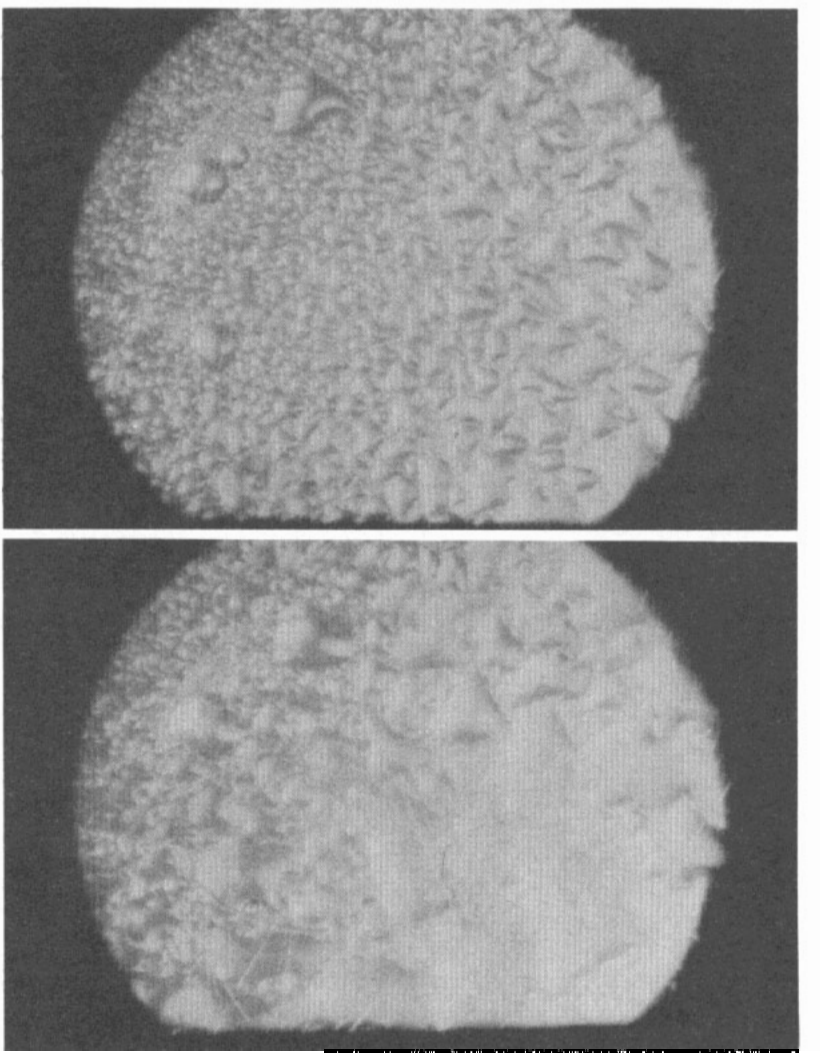

Figure 12. Microphotographs of the growth of the droplets 100 s (upper panel) and 200 s (lower panel) after the cell was closed.

and coalescing and finally producing a continuous film covering the whole solid surface (see figure 12). In order to prevent the effect of gravity on the droplets the sample surface was placed horizontally in all our experiments.

This visual observation confirms that there is in fact formation of droplets on the solid surface and it also explains a feature of the results presented in figure 8: the theory gives results limited to a maximum pressure equal to $P = 21.5$ kPa which corresponds to the saturation for acetone at the temperature of the experiment, a quite normal result since B cannot exist as a gas above this pressure; however, the experiments can be performed well above 21.5 kPa, up to 27.5 kPa.

In fact, knowing that there is formation of droplets that grow and reach macroscopic size, we may conclude that the vapour pressure in the cell is higher than the local saturation

pressure. This effect, called supersaturation, is not taken into account in the theoretical model and so the calculated curves shown in figure 8 do not continue beyond the total pressure corresponding to the saturation of the vapour B.

The conclusion that there is supersaturation when macroscopic droplets develop is based on the following results from thermodynamical studies explaining the dynamics of droplet growth on a solid surface [14]:

(i) if the vapour pressure is smaller than the saturation pressure, only very small droplets are highly probable;

(ii) if the vapour pressure becomes larger than the saturation pressure, the droplet radius can increase indefinitely as soon as it exceeds a few Å. At that moment, macroscopic droplets start to appear. This growth is then spontaneous and does not require any change in the conditions of condensation. In our experiment we noticed, for instance, that if the filling of the cell is stopped at a pressure larger than the saturation pressure, this growth of droplets will not stop.

The effect of this continuous growth on the mirage signal is a signal drift that is particularly evident when we close the cell after reaching supersaturation and then maintain all the experimental parameters constant, including the temperature and the gas pressure in the cell. This effect is clearly observed in figure 13. The amplitude and phase of the mirage signal obtained with a mixture of argon and acetone ($X = 0.9$) and a stainless steel solid sample are recorded as functions of time.

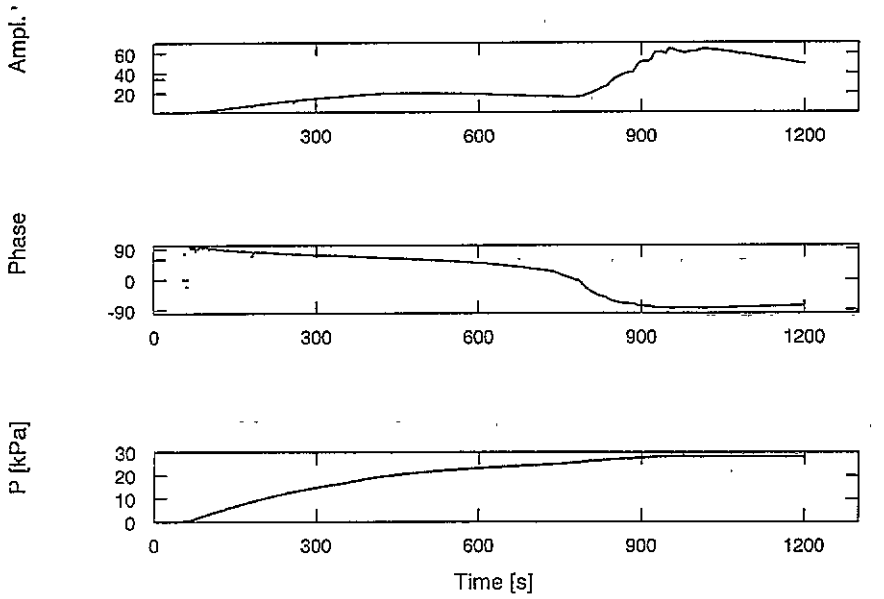

Figure 13. Signal drifts as a function of time during the filling up of the cell with a mixture of acetone ($X = 0.9$) + argon ($T = 269$ K, $z = 190$ mm, $f = 121$ Hz).

Up to 900 s, the pressure (see the curve in the lower part of figure 13) increases in the cell. At this time the cell is closed and the pressure remains constant. The amplitude and phase obtained up to this time are similar to the ones which were described in the previous sections. At $t = 900$ s, the situation corresponds to a supersaturation.

After $t = 900$ s has been reached, the drift of the signal starts: the amplitude decreases and the phase increases which means that the mass contribution decreases. The explanation

of this evolution is that the droplets coalesce when they grow and so while their mean size increases their number is substantially decreased thus decreasing the number of locations on the surface occupied by the triple points (solid–liquid–gas) where the adsorption–desorption induced by the pump takes place. As a consequence the influence of the concentration wave decreases with respect to that of the thermal wave.

The two photographs of the solid surface that we present in figure 12 were taken at time intervals of 100 s after the closing of the cell. They show very clearly the spontaneous growth and coalescence of the droplets under constant experimental conditions, thus confirming the analysis presented in this section.

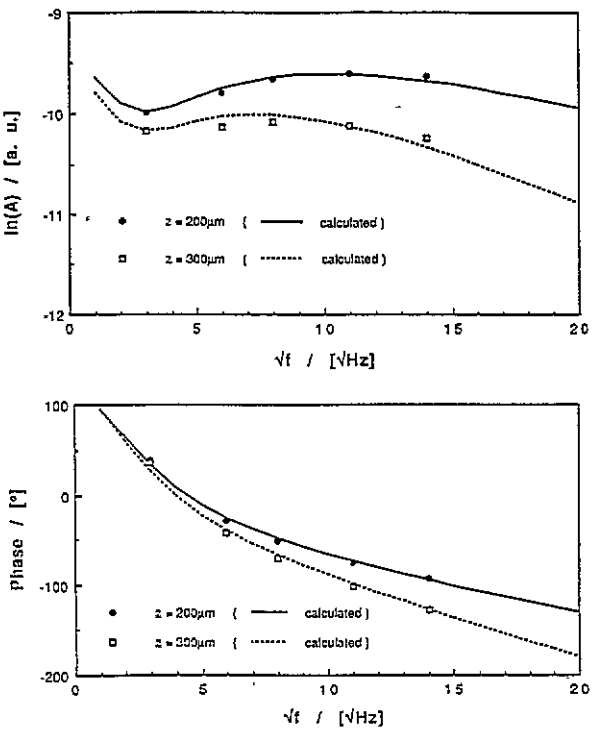

Figure 14. The amplitude and phase versus $f^{1/2}$. The gas mixture was dichloromethane ($X = 0.94$) + argon. $T = 294$ K, $Y_1 = 3 \times 10^{-4}$ mol m^{-2}.

6. Conclusion

Throughout the presentation of these experimental results, three domains appeared as described below.

(i) At low pressures, the thermal contribution dominates. This domain was used to check whether or not the experimental conditions are in agreement with the hypotheses used in the model, such as that of the 1D character of the diffusion or the linearity of the experiment, and to determine the unknown (or poorly known) parameters such as the thermal conductivity of the gas mixture (or the actual concentration in the cell).

(ii) At the other extreme, as the partial pressure of the condensable gas approaches its saturation value the mass contribution becomes more and more important, eventually dominating over the thermal contribution. When supersaturation occurs there is a rapid growth of droplets condensed on the surface. The reduction of the number of these droplets through coalescence produces a decrease of the mass contribution that causes a drift of

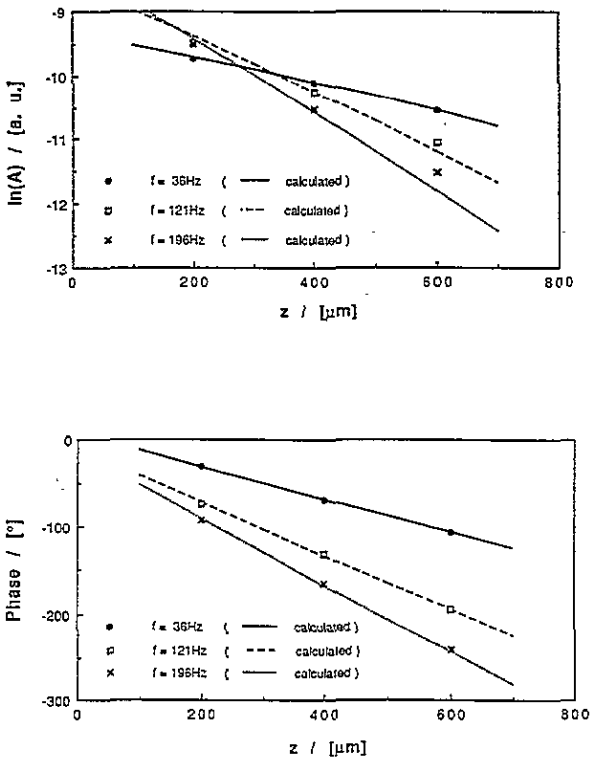

Figure 15. The amplitude and phase versus z for the gas mixture dichloromethane ($X = 0.94$) + argon. $T = 294$ K, $Y_1 = 3 \times 10^{-4}$ mol m^{-2}.

the signal when the filling of the cell is stopped and all experimental parameters are kept constant.

(iii) Since at low pressures the measurements are insensitive to the adsorption process and at high pressures they are subject to non-reproducibility due to the drift, the test of the validity of the model should be performed when the thermal and mass contributions are of the same order of magnitude. Figures 14 and 15 show the results of such a test performed at a pressure that is only a few kPa higher than the pressure producing the minimum of $A(P)$ corresponding to the equality of the two contributions (see the curves for $A(P)$ and $\varphi(P)$ in figure 4, for example). All the theoretical curves in both figures 14 and 15 were obtained using the same values of the thermal, diffusion and adsorption parameters. The quality of the simultaneous fit of these ten curves proves that our model is in very good agreement with the measurements. This agreement also confirms that our experimental conditions are the ones assumed to establish the calculation. Among these hypotheses, let us recall that the system should be in equilibrium, which is certainly not true macroscopically in the experiments. But the mirage probe is so localized and so close to the surface that it actually achieves the measurements in a local equilibrium sufficient to verify the model. This remarkable result is a great advantage of this technique.

Apart from the validation of the theoretical model that we proposed in part I, the goal of this experimental study was to investigate the potential value of the mirage effect for the detection of adsorption–desorption of organic molecules on unprepared surfaces at temperatures and pressures close to NTP. The results presented here demonstrate the good sensitivity of the method to the number of molecules adsorbed in the first layer, i.e. mainly to the surface roughness, and to the ambient conditions of this adsorption, especially surface

temperature. However, the method is not able to test the models of adsorption since we verified that it is insensitive to the formation of the first layer occurring at low pressure, when the thermal contribution dominates.

On the other hand, our study reveals some new important potential applications of the mirage deflection method detailed below.

(i) We were able to confirm experimentally that, as predicted in part I, the mirage method can be used to measure the thermal diffusivity and the mass diffusion coefficient of gas mixtures; since there are currently very few sets of data available on these transport coefficients for gas mixtures, the simplicity and the accuracy of the method that we propose here should make this a new useful application of the mirage deflection technique.

(ii) We found that the mirage method may be used to study the mechanism of the adsorption–nucleation–condensation process and the affinity between condensable materials and any smooth solid surface; however, further investigation is necessary to access more precisely the sensitivity of the mirage method to some important parameters, like the contact angle between the condensate and the solid surface, in order to find out how this method compares with other existing techniques.

(iii) Our experiments reveal the sensivity of the mirage signal to the dynamics of droplet growth on a solid surface; this may be further explored and used to study the mechanisms of droplet growth, including droplet diffusion and coalescence.

Water detection on insulating materials and desorption of organic molecules from painted walls in white rooms could be other interesting potential application areas.

References

[1] Charbonnier F and Fournier D 1986 *Rev. Sci. Instrum.* **57** 1126
[2] Charbonnier F, Lepoutre F, Roger J P, Fournier D, Boccara A C, Lemoine A and Robert P 1988 *Review of Progress in Quantitative Nondestructive Evaluation* vol 8A, ed D O Thompson and D Chimenti (New York: Plenum) p 1105
[3] See, for instance,
Aamodt L C and Murphy J C 1981 *J. Appl. Phys.* **52** 4903
[4] McDonald F A and Wetsel G C 1988 *Physical Acoustics* vol 18 (New York: Academic) p 167
[5] Opsal J, Rosencwaig A and Willenborg D L 1983 *Appl. Opt.* **22** 3169
[6] Kuo P K, Inglehart L J, Sendler E D, Lin M J, Favro L D and Thomas R L 1984 *Review of Progress in Quantitative Nondestructive Evaluation* vol 4B, ed D O Thompson and D Chimenti (New York: Plenum) p 745
[7] Rousset G, Lepoutre F and Bertrand L 1983 *J. Appl. Phys* **54** 2383
[8] Surnev S and Ivanov D 1990 *Revue Phys. Appl.* **25** 457
[9] Rollat N 1988 *Thèse de Doctorat* Université de Paris 6
[10] Ganguly P and Somasundaram T 1987 *Appl. Phys.* B **43** 43
[11] Rudzinski W and Everett D H 1992 *Adsorption of Gases on Heterogeneous Surfaces* (London: Academic)
[12] Adamson A W 1982 *Physical Chemistry of surfaces* (New York: Wiley)
[13] Steyer A, Guenoun P and Beysens D 1992 *Phys. Rev. Lett.* **68** 64
[14] Steyer A 1991 *Thèse de Doctorat* Université de Paris 6